Electronic phase diagram of $NdFe_{1-x}Rh_xAsO$

David Bérardan, Lidong Zhao, Loreynne Pinsard-Gaudart, and Nita Dragoe
Institut de Chimie Moléculaire et des Matériaux d'Orsay, UMR CNRS 8182, Bât. 410, Univ. Paris-Sud 11, 91405 Orsay, France
(Received 16 December 2009; revised manuscript received 9 February 2010; published 5 March 2010)

We report on the electrical resistivity, thermoelectric power, and electronic phase diagram of rhodium-doped NdFeAsO. Rhodium doping suppresses the structural phase transition and spin-density wave observed in the undoped material, and superconductivity emerges at x close to 0.05, despite the distortion of $FeAs_4$ tetrahedra induced by the large size difference between Rh and Fe elements. The $T_c(x)$ curve is domelike, and the highest T_c is reached at $x=0.1$, with $T_c^{onset}=18$ K. An upturn of the electrical resistivity above T_c has been observed, with a Kondo-type behavior above T_c and a Fermi-liquid behavior close to room temperature.

DOI: 10.1103/PhysRevB.81.094506 PACS number(s): 74.70.Xa, 74.25.fg, 74.25.Dw, 74.62.Dh

I. INTRODUCTION

Since the discovery of superconductivity at 26 K in $LaFeAsO_{1-x}F_x$ ("1111" compounds) in 2008,[1] an intense research activity has emerged dealing with the study of the oxypnictides, a new family of high-T_c superconductors outside the cuprates family. In a matter of months after the first report of Kamihara *et al.*, the critical temperature of these compounds has been raised to over 50 K by replacing lanthanum by smaller rare-earth elements.[2] For a recent review about the superconductivity in this materials family, see Ref. 3.

The parent compound LaFeAsO, which consists in alternating La_2O_2 and Fe_2As_2 layers, is not superconducting but it exhibits a metallic behavior with a structural transition from tetragonal to orthorhombic as well as a spin-density wave (SDW), both emerging around 150 K.[4] Upon doping, the structural transition and the spin-density wave are both destroyed and a superconducting state is observed.[4] This superconducting state can be induced by electron doping, with fluorine doping[1] or oxygen-vacancies formation[5] on the oxygen site, or with thorium doping on the rare-earth site.[2] It can also emerge from a hole doping with strontium on the rare-earth site.[6] More surprisingly, it has been shown that in addition to the electron or hole doping in the La_2O_2 layers, a partial substitution of iron by cobalt[7] or nickel[8] in the Fe_2As_2 layers also leads to the emergence of superconductivity, which is very different from the cuprates behavior where the superconducting state is very sensitive to the presence of impurities on the copper site. Indeed, the electronic phase diagram proposed by Wang *et al.* for $LaFe_{1-x}Co_xAsO$ exhibits a domelike curve for T_c as a function of Co content,[9] which resembles that of $LaFeAsO_{1-x}F_x$.[1] However, it seems that hole doping cannot be induced by substitutions in the Fe_2As_2 layers.[10,11] Recently, Lee *et al.* have reported the effect of Ru doping in optimally doped $NdFeAsO_{0.89}F_{0.11}$.[12] These authors showed that the rate of T_c decrease induced by Ru doping is very small, despite the structural distortion induced by the doping. Moreover, we have shown that despite the large size difference between Fe and Rh elements, superconductivity can be induced by rhodium doping in NdFeAsO.[13] In this paper, we report on the transport properties and the electronic phase diagram of $NdFe_{1-x}Rh_xAsO$.

II. EXPERIMENTAL

Samples with nominal composition $NdFe_{1-x}Rh_xAsO$ ($0.025<x<0.20$) were prepared by a solid-state reaction route, using Nd, As, Fe, and Rh metals and Fe_2O_3 powder. All handlings were made in an Ar-filled glove box with less than 1 ppm O_2 and H_2O. NdAs alloy was first obtained by heating Nd and As under pure Ar in a closed silica tube at 900 °C. The single phase nature of the alloy was confirmed by x-ray diffraction (XRD). NdAs was then carefully mixed in stoichiometric ratio with Fe, Fe_2O_3, and Rh, and the resulting powder was pressed into $2\times3\times12$ mm^3 bars under 200 MPa. These bars were heated two times with intermediate grinding and pressing, at 1150 °C during 48 h under argon in closed silica tubes. X-ray diffraction characterization was performed using a Panalytical X'Pert diffractometer with a Ge(111) incident monochromator and a X'celerator detector. The XRD patterns were analyzed using the Rietveld method with the help of the FULLPROF software.[14] The thermoelectric power was measured by a differential method with two T-type thermocouples, by using the slope of the ΔV-ΔT curve with thermal gradients along the samples up to about 0.3 K/mm, in a laboratory made system. The electrical resistivity was obtained between 2 and 300 K and between 0 and 9 T by a dc four wires method using a Quantum Design physical properties measurement system (PPMS) and silver paste for the electrical contacts. All transport measurements were performed in a direction perpendicular to the pressing direction. Magnetic susceptibility was measured down to 5 K using a Quantum Design magnetic properties measurement system (MPMS) under 20 Oe.

III. RESULTS AND DISCUSSION

Figure 1 shows the XRD patterns of $NdFe_{1-x}Rh_xAsO$ compounds ($x=0.025-0.2$). All major Bragg peaks can be indexed using a tetragonal unit cell with structure-type ZrCuSiAs,[15] represented in the inset of Fig. 2, indicating that the samples are almost single phase. An example of Rietveld refinement is shown in Fig. 2, which also shows the positions of the Bragg reflexions of the 1111 phase. The typical R values for all the refinements are $R_F\sim3\%$, $R_{Bragg}\sim3\%$, and $R_{wp}\sim12\%$. Less than 3% secondary phase is observed, which corresponds to $Nd(OH)_3$, that results from Nd_2O_3 mi-

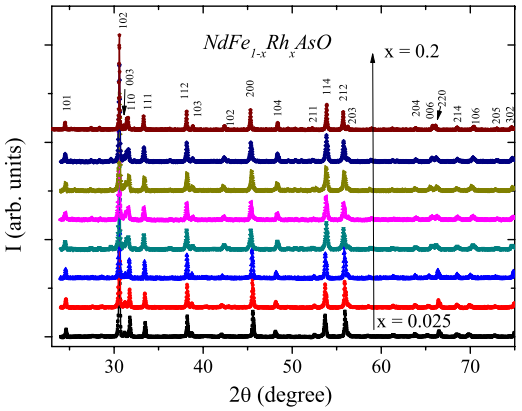

FIG. 1. (Color online) XRD patterns of $NdFe_{1-x}Rh_xAsO$ compounds with x=0.025 (bottom) to x=0.2 (top).

nority phase under air. A partial preferential orientation of the grains along the [0 0 1] direction has been observed, which is related to the microstructure of these compounds and most probably originates from the uniaxial pressing of the powder.

The structural parameters determined using the Rietveld refinements are summarized in Fig. 3 as a function of the rhodium fraction. A significant increase in a is observed with increasing rhodium fraction, which is consistent with the atomic radius of Rh being larger than that of Fe.[16] This linear trend confirms that the substitution of iron by rhodium in the NdFeAsO unit cell occurs. Despite the increase in the lattice parameter a with increasing Rh fraction, the unit-cell volume is almost unaffected by the substitution, due to the simultaneous decrease in c that results in a reduced interlayer distance. Schematically, the NdFeAsO unit cell can be pictured as alternating $[Nd_2O_2]^{2+}$ and $[Fe_2As_2]^{2-}$ layers (see Fig. 2). The substitution of iron by rhodium leads to an increase in the electrons density in the metal-pnictide layer following $[Fe_{2-2x}Rh_xAs_2]^{(2+2x)-}$, which increases the interlayer Coulomb attraction and decreases the interlayer distance and therefore the lattice parameter c. A similar behavior has already been reported in Co-doped LaFeAsO, where the substitution of iron by cobalt leads to a strong decrease in the c parameter whereas a remains almost unchanged.[7,9] This increase in the carriers concentration with Rh doping is confirmed by our thermoelectric power measurements, see later. Due to the simultaneous decrease in c and increase in a, the distortion of the $FeAs_4$ tetrahedra increases. As can be seen in Fig. 3, the difference between the two characteristic As-FeAs angles of the $FeAs_4$ tetrahedra increases gradually with the rhodium substitution. On the contrary, fluorine doping leads to a decrease in the distortion of the tetrahedral as compared to NdFeAsO.

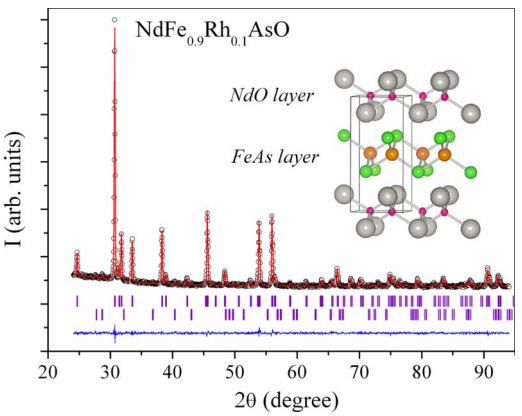

FIG. 2. (Color online) XRD pattern and Rietveld refinement of $NdFe_{0.9}Rh_{0.1}AsO$. Minor impurity peaks correspond to $Nd(OH)_3$. The crystal structure is also plotted showing the FeAs and NdO layers (inset).

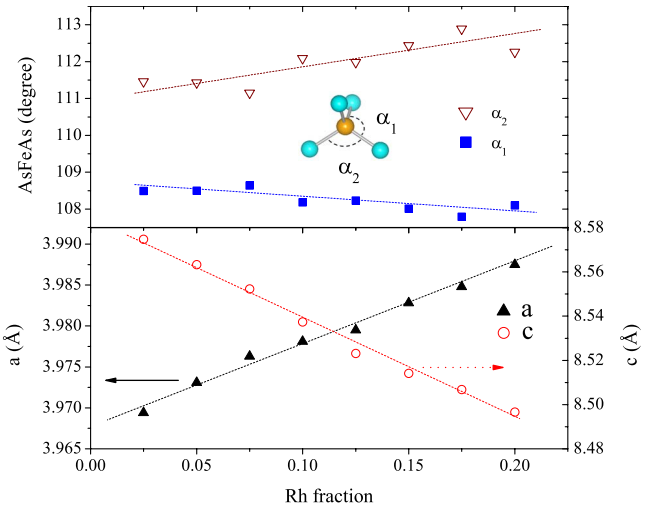

FIG. 3. (Color online) Evolution with the rhodium fraction in $NdFe_{1-x}Rh_xAsO$ of the lattice parameters (bottom) and of the angles of the $FeAs_4$ tetrahedra (top). Lines are visual guides.

Figure 4 shows the temperature dependence of the electrical resistivity in the series $NdFe_{1-x}Rh_xAsO$ normalized to the room-temperature values. The undoped parent compound is known to exhibit a strong anomaly of the electrical resistivity around 150 K followed by a large decrease in the resistivity at lower temperature (see, for example, Ref. 17). Upon doping with 2.5 at. % rhodium, the anomaly shifts to a lower temperature ($T_{anom} \sim 95$ K) and becomes less pronounced. The origin of this anomaly is probably the same as

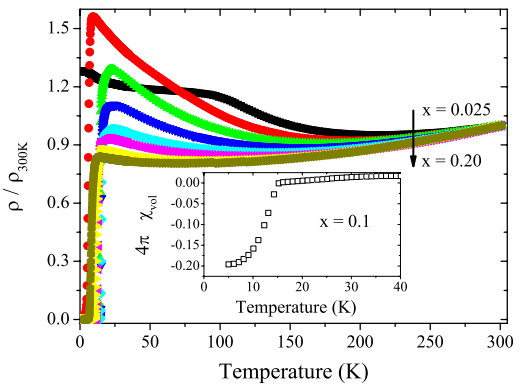

FIG. 4. (Color online) Temperature dependence of the normalized electrical resistivity in the series $NdFe_{1-x}Rh_xAsO$. Inset: temperature dependence of the magnetic susceptibility of $NdFe_{0.9}Rh_{0.1}AsO$ recorded in a zero-field-cooled mode at 20 Oe.

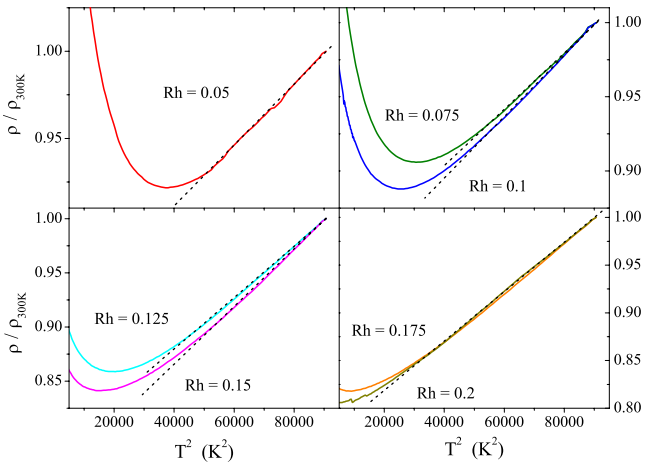

FIG. 5. (Color online) Temperature dependence of the normalized electrical resistivity in the series $NdFe_{1-x}Rh_xAsO$, temperature scale in T^2. The black dashed lines are linear fits.

is the undoped compound, where it has been attributed to a SDW and a structural transition from tetragonal at room temperature to orthorhombic at low temperature. With a further increase in the rhodium fraction ($x>0.05$), no anomaly can be observed any longer, and an unambiguous superconducting transition emerges at low temperature. The inset of Fig. 4 shows the volumic magnetic susceptibility of $NdFe_{0.9}Rh_{0.1}AsO$, which exhibits the highest T_c in the series, obtained in a zero-field-cooled mode with an excitation field of 20 Oe, assuming a sample density equal to the theoretical one. A superconducting transition can be observed around 15 K. From the diamagnetic signal at 5 K, the shielding fraction can be estimated to about 20% of the volume of the sample, which confirms the bulk nature of the superconductivity.

The highest critical temperature observed in the $NdFe_{1-x}Rh_xAsO$ series, $T_c^{onset}\sim 18$ K, is much lower than the one observed in $NdFeAsO_{0.88}F_{0.12}$.[18] A similar difference has already been reported between fluorine-doped and cobalt-doped LnFeAsO.[1,9] Lee *et al.* have suggested that the highest T_c is obtained when the Fe_2As_2 lattice forms regular tetrahedra.[19] Our results are consistent with this picture, with $FeAs_4$ tetrahedra being more distorted and T_c being lower with Rh doping than with F doping. However, the maximum critical temperature observed in $NdFe_{0.9}Rh_{0.1}AsO$ is much lower that the one that would be expected using the T_c vs α_2 dependence suggested in Ref. 19, which should be closer to 30 K.

Two significant differences between the temperature dependence of the electrical resistivity of the fluorine-doped sample[18] and of the rhodium-doped ones (Fig. 4) can be underlined.

First, although both fluorine-doped and rhodium-doped samples exhibit a metallic electrical resistivity close to room temperature, the temperature dependence of the resistivity is different. $NdFeAsO_{0.88}F_{0.12}$ behaves like a "strange metal" with the exponent x of $\rho\sim T^x$ that changes from $x>1$ to $x<1$ when the temperature exceeds about 150 K.[20,21] On the other hand, rhodium-doped samples exhibit a Fermi-liquid behavior with $\rho\sim\rho_0+AT^2$, which evidences enhanced electron-electron interactions. Figure 5 shows the temperature dependence of the normalized electrical resistivity in the series $NdFe_{1-x}Rh_xAsO$, with the temperature scale in T^2. A linear trend can be observed for every sample above 200–220 K ($0.05<x<0.2$). These observations, which are in good agreement with the results reported in the series $LaFe_{1-x}Ni_xAsO$,[22] are not fully consistent with the electronic phase diagram suggested by Hess *et al.*[23] for FeAs superconductors, who indicated that the Fermi-liquid behavior should be a characteristic feature of the overdoped regime.

Second, for the fluorine-doped sample, the resistivity in the normal state is typical of a metal from T_c to room temperature. On the contrary, in the rhodium-doped compounds, whereas the resistivity is also metallic around room temperature, a minimum can be observed at T_{min} followed by an upturn of the resistivity that exhibits a semiconductorlike behavior between T_{min} and T_c ($0.05<x<0.2$). The temperature of the minimum of the resistivity T_{min} shifts to lower temperatures when the rhodium fraction is increased. Moreover, the maximum of resistivity above T_c becomes less pronounced for higher Rh fractions. A similar behavior has already been reported in Ni-doped[8] and Co-doped LnFeAsO.[7,9] A much less pronounced upturn of the resistivity has also been reported in some F-doped LaFeAsO samples with small fluorine content[1] whereas it does not seem to be present in optimally doped samples or other rare earth than lanthanum (Refs. 18 and 22–24). At the first glance, it seems that this metallic to semiconductorlike transition could be simply explained by the local structural disorder induced in the conducting Fe_2As_2 layer by rhodium doping. With increasing rhodium fraction, the increased carriers' concentration would lead to a more metallic behavior that would eventually hide the upturn. However, this simple picture is not consistent with the results recently published by Lee *et al.*[12] These authors reported the effects of ruthenium doping on the electrical transport behavior of fluorine-doped $NdFeAsO_{0.89}F_{0.11}$. Whatever the Ru fraction, no maximum of the resistivity has been observed and all $NdFe_{1-y}Ru_yAsO_{0.89}F_{0.11}$ samples are metallic above T_c, which seems to rule out the possible role of the structural disorder. Moreover, this upturn cannot be linked to thermal excitation of carriers through a band gap, as band-structure calculations and photoemission spectroscopy experiments have unambiguously proved the metallic nature of this family of compounds (see, for example, Ref. 24).

Recently, Cao *et al.* have suggested that the resistivity upturn above T_c could originate from Kondo effect.[22,25] In their picture, Ni doping in the Fe_2As_2 layer of LaFeAsO not only induces itinerant carriers but also stabilized localized moment, in agreement with band-structure calculations.[26] Indeed, the coexistence of itinerant charge carriers and local moments and a resistivity upturn following a $\log(T)$ behavior is often characteristic of Kondo effect.[27] A similar $\log(T)$ dependence of the normal-state resistivity as also be observed by Tropeano *et al.* in $Fe_{1+x}Te_{1-x}Se_x$,[28] coupled to a B^2 dependence of the magnetoresistivity. Moreover, the temperature dependence of the reported magnetoresistivity is well described using a Kondo formalism. In this latter case, the magnetic impurities originate from the excess of Fe, which provides localized magnetic moments.[29,30]

Figure 6 shows the temperature dependence of the normalized electrical resistivity in the $NdFe_{1-x}Rh_xAsO$ series,

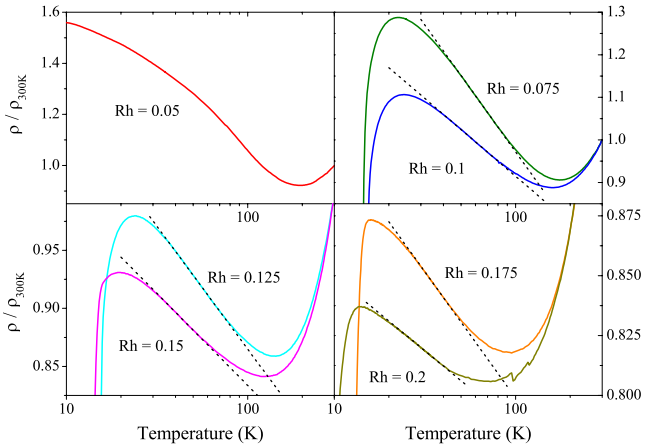

FIG. 6. (Color online) Temperature dependence of the normalized electrical resistivity in the series $NdFe_{1-x}Rh_xAsO$, temperature scale in $\log(T)$. The black dashed lines are linear fits.

with the temperature scale in $\log(T)$. Although no linear trend can be observed with $x=0.05$ in any temperature range, all samples with $x>0.075$ exhibit a linear behavior in a narrow temperature range (black dashed lines). The absence of linear behavior with $x=0.05$ could be connected to a reminiscence of the spin-density wave, as this compound lies close to the boundary of the superconducting area of the phase diagram. The width of this $\log(T)$ area decreases with increasing Rh fraction, from about 65 K with $x=0.075$ to about 25 K with $x=0.2$. This decrease is connected to the electron doping induced by the substitution of Fe by Rh. Indeed, band-structure calculations have shown that the density of states at the Fermi level $N(E_F)$ is reduced upon doping in the LnFeAsO system.[26] As the Kondo temperature decreases when $N(E_F)$ decreases, increasing Rh fraction leads to a decrease in T_{min}. The upturn of the electrical resistivity above T_c is more pronounced in Rh-doped samples than in the F-doped ones (where it is not always present) because the substitution of iron by rhodium increases not only the carrier concentration but could also induce the presence of local moments in the Fe_2As_2 layer, similarly to Ni doping in LaFeAsO or Fe excess in $FeTe_{1-x}Se_x$, which in turn increases the electrons scattering rate. This observation is also consistent with the highest observed T_c^{onset} being lower than the one expected considering the distortion of the $FeAs_4$ tetrahedra, as the local moments induced by Rh doping could also act as pair breaker and lower the critical temperature. Nevertheless, the resistivity upturn above T_c could also originate from weak-localization effects linked to the two-dimensional character of this material, and no definitive conclusion can be drawn at the moment.

An electronic phase diagram of the series $NdFe_{1-x}Rh_xAsO$ based on the electrical resistivity data is plotted in Fig. 7. The SDW area is very narrow. The frontier is not well defined and from our data, it is not clear if there is coexistence of the SDW and of superconductivity in $NdFe_{0.95}Rh_{0.05}AsO$. For Rh fractions higher than 0.05, the SDW is clearly suppressed, and a superconducting state emerges at low temperature, with a domelike T_c(Rh) curve, characteristic of the FeAs superconductors. Although the de-

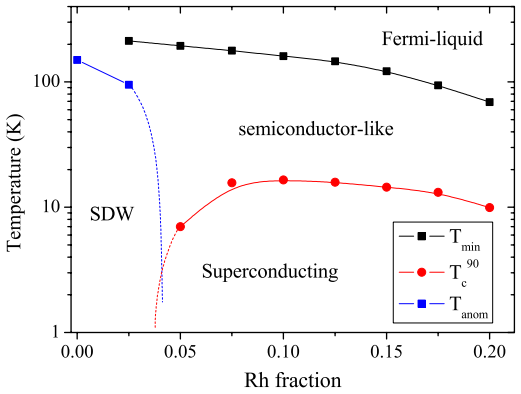

FIG. 7. (Color online) Electronic phase diagram for $NdFe_{1-x}Rh_xAsO$ (vertical axis is in logarithmic scale). The point at $x=0$ is taken from Ref. 19.

tails are different, this domelike evolution is similar to the one reported for Co-doped LnFeAsO.[7,9] However, contrary to the Co-doped systems, superconductivity is not destroyed up to $x>0.2$. For $x>0.075$, the normal-state resistivity exhibits a Fermi-liquid behavior close to room temperature, that changes to a "Kondo-type" temperature dependence above T_c, with T_{min} that decreases with increasing rhodium fraction.

We have compared the temperature dependence of the electrical resistivity under several magnetic fields up to 9 T for $NdFe_{0.9}Rh_{0.1}AsO$, which exhibits the highest-T_c value in the $NdFe_{1-x}Rh_xAsO$ series, in order to estimate the upper critical field H_{c2}. All curves are plotted in Fig. 8. T_c^0 corresponds to the zero resistivity temperature, defined as the temperature where the resistivity goes below the sensibility limit of the PPMS. As can be seen in Fig. 8, T_c^{90} decreases very weakly with the magnetic field whereas T_c^0 decreases more rapidly leading to a widening of the superconducting transition, characteristic of type II superconductivity (the field dependence of T_c^0 and T_c^{90} are plotted in the inset of Fig. 8). It is noteworthy that T_c^0 is still higher than 4 K even under a magnetic field as high as 9 T, which evidences the very robust character of the superconducting state in this family of materials. Without magnetic field, the width of the superconducting transition is small. If we define ΔT_c as $T_c^{90}-T_c^{10}$, ΔT_c

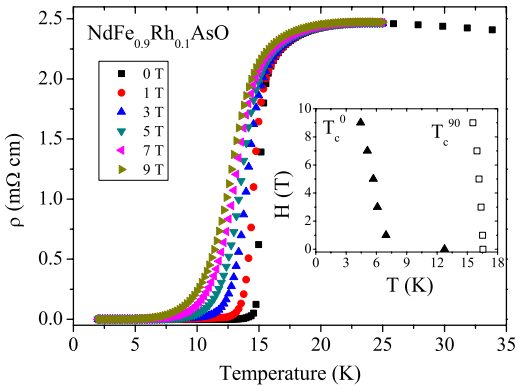

FIG. 8. (Color online) Field dependence of the superconducting transition in $NdFe_{0.9}Rh_{0.1}AsO$. Inset: field dependence of T_c^{90} and T_c^0.

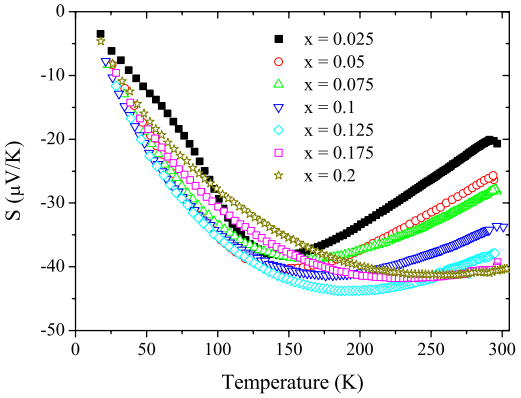

FIG. 9. (Color online) Temperature dependence of the thermoelectric power in the series $NdFe_{1-x}Rh_xAsO$.

is a low as 1.8 K, which is much smaller than the value reported for cobalt doped LaFeAsO (Ref. 7) or that the one of fluorine-doped NdFeAsO.[31]

The slope $(dH_{c2}/dT)_{|T=T_c}$ for T_c^{90} is about -9 T K^{-1}. Using the Werthamer-Helfand-Hohenberg formula $H_{c2}(0)=-0.693\ T_c\ (dH_{c2}/dT)_{|T=T_c}$ leads to H_{c2} (0) on the order of 100 T, which is much higher than the values reported for Co-doped LnFeAsO,[7,32] and of the same order as the value of $NdFeAsO_{0.88}F_{0.12}$.[31]

In the superconducting 1111 compounds, a peak of the thermoelectric power above T_c has been widely reported (see, for example, Ref. 33 and 34). Wang *et al.* have suggested that this enhancement of the thermoelectric power in superconducting compounds could be somehow correlated with the onset of superconductivity.[9] Figure 9 shows temperature dependence of the thermoelectric power in the series $NdFe_{1-x}Rh_xAsO$. All samples are *n* type, which is consistent with an increase in the electrons concentration induced by the substitution of Fe by Rh. Band-structure calculations have shown that 1111 compounds are multiband materials, and that several electron and hole pockets contribute to the electrical transport.[35] In a multiband system, the thermoelectric power is a mixture of the individual thermoelectric power of each contributing band following

$$S_{tot} = \frac{\Sigma \sigma_i S_i}{\Sigma \sigma_i}$$

with σ_i and S_i being, respectively, the conductivity of the *i*th band and its contribution to the thermoelectric power (negative for an electron band and positive for a hole band). The thermoelectric power of undoped NdFeAsO has been reported by McGuire *et al.*[17] Below about 150 K, the thermoelectric power is dominated by hole pockets and is positive. Then a sharp transition occurs at about 150 K, with denotes a strong evolution of the conduction mechanism with the structural transition and the emergence of the spin-density wave. Above 150 K, the thermoelectric power is negative up to room temperature. When iron is substituted by rhodium, the hole pockets are gradually suppressed, and the thermoelectric power becomes *n* type in the whole temperature range. Although the sign of the thermoelectric power does

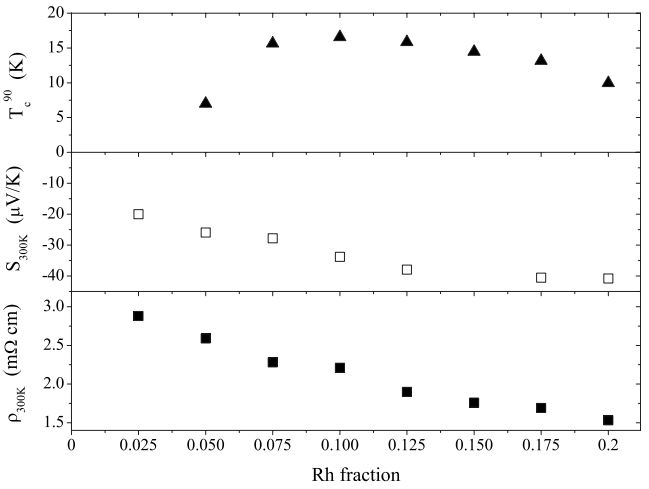

FIG. 10. Evolution of the room-temperature electrical resistivity (bottom), thermoelectric power (middle), and critical temperature T_c^{90} with the rhodium fraction in $NdFe_{1-x}Rh_xAsO$.

not change, a reminiscence of the transition between electron-dominated and hole-dominated thermoelectric power can still be observed for $x=0.025$. When the rhodium fraction is increased further, no feature (transition, bump, or kink) can be observed and the temperature dependence of the thermoelectric power gradually approaches that of a metal. This evolution can also be explained by considering a gradual suppression of the hole pockets and therefore a decrease in the "positive" contributions to the total thermoelectric power.

If we compare the thermoelectric power of F-doped samples[33] and that of Rh-doped samples, it is noteworthy that no significant peak can be observed above T_c in superconducting $NdFe_{1-x}Rh_xAsO$ samples (see, for instance, $x=0.1$ and $x=0.125$, which correspond to the highest observed T_c). This behavior is also slightly different from the one observed for Co-doped LnFeAsO.[7,9] Therefore, it seems that the electronic band structure is influenced by Rh doping as compared to F or Co doping.

In order to compare the behavior of T_c and S of Rh-doped samples to the ones of Co-doped samples as reported by Wang *et al.*,[9] the evolution with the rhodium fraction of T_c^{90}, the room-temperature thermoelectric power and the room-temperature resistivity have been plotted in Fig. 10. No obvious link can be seen between the critical temperature and the thermoelectric power, and no anomalous enhancement of the thermoelectric power in the superconducting window can be seen. Therefore, this enhancement does not seem to be an universal feature of iron-based arsenic superconductors. However, the evolutions of the room-temperature values of the resistivity and of the thermoelectric power can both be well explained taking into account an increase in the electrons concentration in the system due to rhodium doping. This raises into question the origin of the abnormal contribution to the thermoelectric power in F-doped iron pnictides.

IV. CONCLUSION

To sum up, our systematic study of the electrical transport properties in the series $NdFe_{1-x}Rh_xAsO$ have lead to estab-

lish the electronic phase diagram of Rh-doped NdFeAsO. The evolution with rhodium doping of the thermoelectric power as well as the room-temperature value of the electrical resistivity indicates that rhodium doping on the iron site first leads to a suppression of the hole pockets at the Fermi level and then to an increase in the electrons concentration. The spin-density wave and the structural transition are suppressed by Rh doping and a superconducting state emerges for a rhodium fraction close to 0.05. Rh-doped NdFeAsO compounds exhibit a domelike dependence of T_c, similar to F-doped compounds, although the highest value of T_c is much lower with Rh doping. This difference can be well explained taking into account both the distortion of the $FeAs_4$ tetrahedra and the pair-breaking effect of localized moments in the Fe_2As_2 layer induced by Rh doping. These localized moments also possibly induce a scattering of the electrons above T_c leading to a Kondo-type behavior of the electrical resistivity, which is not observed in F-doped NdFeAsO, although no definitive conclusion about the resistivity upturn can be provided at the moment. Close to room temperature, $NdFe_{1-x}Rh_xAsO$ compounds exhibit a Fermi-liquid behavior, which denotes strong electron-electron interactions.

ACKNOWLEDGMENTS

This work was supported by the *Triangle de la Physique*, project STP 2008-095T. The authors acknowledge E. Rivière for SQUID measurements, F. Bouquet for his help with PPMS measurements, and C. Godart for a gift of rhodium powder.

[1] Y. Kamihara, T. Wanatabe, M. Hirano, and H. Hosono, J. Am. Chem. Soc. **130**, 3296 (2008).
[2] C. Wang, L. Li, S. Chi, Z. Zhu, Z. Ren, Y. Li, Y. Wang, X. Lin, Y. Luo, S. Jiang, X. Xu, G. Cao, and Z. Xu, EPL **83**, 67006 (2008).
[3] K. Ishida, Y. Nakai, and H. Hosono, J. Phys. Soc. Jpn. **78**, 062001 (2009).
[4] C. de la Cruz, Q. Huang, J. W. Lynn, J. Li, W. Ratcliff, II, J. L. Zarestky, H. A. Mook, G. F. Chen, J. L. Luo, N. L. Wang, and P. Dai, Nature (London) **453**, 899 (2008).
[5] Z.-A. Ren, G.-C. Che, X.-L. Dong, J. Yang, W. Lu, W. Yi, X.-L. Shen, Z.-C. Li, L.-L. Sun, F. Zhou, and Z.-X. Zhao, EPL **83**, 17002 (2008).
[6] H.-H. Wen, G. Mu, L. Fang, H. Yang, and X. Zhu, EPL **82**, 17009 (2008).
[7] A. S. Sefat, A. Huq, M. A. McGuire, R. Jin, B. C. Sales, D. Mandrus, L. M. D. Cranswick, P. W. Stephens, and K. H. Stone, Phys. Rev. B **78**, 104505 (2008).
[8] Y. K. Li, X. Li, T. Zhou, J. Q. Shen, Q. Tao, G. H. Cao, and Z. A. Xu, J. Phys.: Condens. Matter **21**, 355702 (2009).
[9] C. Wang, Y. K. Li, Z. W. Zhu, S. Jiang, X. Lin, Y. K. Luo, S. Chi, L. J. Li, Z. Ren, M. He, H. Chen, Y. T. Wang, Q. Tao, G. H. Cao, and Z. A. Xu, Phys. Rev. B **79**, 054521 (2009).
[10] D. Bérardan, L. Pinsard-Gaudart, and N. Dragoe, J. Alloys Compd. **481**, 470 (2009).
[11] Y. Tsukamoto, Y. Okamoto, and Z. Hiroi, Physica C (to be published 2009).
[12] S. Lee, E. Satomi, Y. Kobayashi, and M. Sato, J. Phys. Soc. Jpn. **79**, 023702 (2010).
[13] D. Bérardan, L. Zhao, L. Pinsard-Gaudart, and N. Dragoe, Physica C **470**, 165 (2010).
[14] J. Rodriguez-Carvajal, Physica B **192**, 55 (1993).
[15] P. Quebe, L. J. Terbüchte, and W. Jeitschko, J. Alloys Compd. **302**, 70 (2000).
[16] R. D. Shannon, Acta Crystallogr.,Sect. A: Cryst. Phys., Diffr., Theor. Gen. Crystallogr. **32**, 751 (1976).
[17] M. A. McGuire, R. P. Hermann, A. S. Sefat, B. C. Sales, R. Jin, D. Mandrus, F. Grandjean, and G. J. Long, New J. Phys. **11**, 025011 (2009).
[18] Z. A. Ren, J. Yang, W. Lu, W. Yi, X.-L. Shen, Z.-C. Li, G.-C. Che, X.-L. Dong, L.-L. Sun, F. Zhou, and Z.-X. Zhao, EPL **82**, 57002 (2008).
[19] C.-H. Lee, A. Iyo, H. Eisaki, H. Kito, M. T. Fernandez-Diaz, T. Ito, K. Kihou, H. Matsuhata, M. Braden, and K. Yamada, J. Phys. Soc. Jpn. **77**, 083704 (2008).
[20] P. Cheng, H. Yang, Y. Jia, L. Fang, X. Zhu, G. Mu, and H.-H. Wen, Phys. Rev. B **78**, 134508 (2008).
[21] H. Q. Luo, P. Cheng, Z. S. Wang, H. Yang, Y. Jia, L. Fang, C. Ren, L. Shan, and H.-H. Wen, Physica C **469**, 477 (2009).
[22] G. Cao, S. Jiang, X. Lin, C. Wang, Y. Li, Z. Ren, Q. Tao, C. Feng, J. Dai, Z. Xu, and F. C. Zhang, Phys. Rev. B **79**, 174505 (2009).
[23] C. Hess, A. Kondrat, A. Narduzzo, J. E. Hamann-Borrero, R. Klingeler, J. Werner, G. Behr, and B. Büchner, EPL **87**, 17005 (2009).
[24] A. Koitzsch, D. Inosov, J. Fink, M. Knupfer, H. Eschrig, S. V. Borisenko, G. Behr, A. Köhler, J. Werner, B. Büchner, R. Follath, and H. A. Dürr, Phys. Rev. B **78**, 180506(R) (2008).
[25] J. Dai, G. Cao, H. Wen, and Z. Xu, arXiv:0901.2787 (unpublished).
[26] G. Xu, W. Ming, Y. Yao, X. Dai, S.-C. Zhang, and Z. Fang, EPL **82**, 67002 (2008).
[27] A. C. Hewson, *The Kondo Problem to Heavy Fermions* (Cambridge University Press, New York, 1997).
[28] M. Tropeano, I. Pallecchi, M. Cimberle, C. Ferdeghini, G. Lamura, M. Vignolo, A. Martinelli, A. Palenzona, and M. Putti, arXiv:0912.0395 (unpublished).
[29] S. Li, C. de la Cruz, Q. Huang, Y. Chen, J. W. Lynn, J. Hu, Y.-L. Huang, F.-C. Hsu, K.-W. Yeh, M.-K. Wu, and P. Dai, Phys. Rev. B **79**, 054503 (2009).
[30] L. J. Zhang, D. J. Singh, and M.-H. Du, Phys. Rev. B **79**, 012506 (2009).
[31] J. Jaroszynski, F. Hunte, L. Balicas, Y.-j. Jo, I. Raičević, A. Gurevich, D. C. Larbalestier, F. F. Balakirev, L. Fang, P. Cheng, Y. Jia, and H. H. Wen, Phys. Rev. B **78**, 174523 (2008).
[32] J. Prakash, S. J. Singh, S. Patnaik, and A. K. Ganguli, Solid State Commun. **149**, 181 (2009).
[33] L. Pinsard-Gaudart, D. Bérardan, J. Bobroff, and N. Dragoe, Phys. Status Solidi (RRL) **2**, 185 (2008).
[34] A. S. Sefat, M. A. McGuire, B. C. Sales, R. Jin, J. Y. Howe, and D. Mandrus, Phys. Rev. B **77**, 174503 (2008).
[35] D. J. Singh and M.-H. Du, Phys. Rev. Lett. **100**, 237003 (2008).